Electrostatic Thrusters for Microgravity Propulsion in a Pressurized Environment

Electrostatic Thrusters for Microgravity Propulsion in a Pressurized Environment

Alvar Saenz-Otero, Alex Pina, Gregory Wellman, Paulo Lozano
MIT Space Systems Laboratory
77 Massachusetts Ave
Cambridge, MA 02139
617-324-6827
alvarso@mit.edu

Richard Garriott
Space Adventures
rgarriott@spaceadventures.com

Abstract — Motivated by long-term human exploration missions which could benefit from robotic assistants, a prototype thruster based on an Ion-Drag Pump was developed. This thruster utilizes no consumable propellant. Its operated by ionizing the air it floats in. Such an engine only requires recharging of its electrical power in order to propel itself in a pressurized microgravity environment. The prototypes were modeled analytically in 1D, tested using a micro-scale, and then validated in 3D aboard the ZERO-G reduced gravity aircraft. The results demonstrated that an engine with an inlet area of 5cm^2 and a needle density of 1.0 needles/cm^2 can provide a thrust of at least 3mN with electrical inputs of 10kV and less than 100uA. The successful demonstration is a proof of concept and opens the possibility for future engines that could provide the desired thrust to support astronauts.[1,2]

TABLE OF CONTENTS

1. INTRODUCTION

The long-term presence of humans in space can benefit substantially from the availability of an autonomous vehicle which operates inside a pressurized vessel, especially if , it does not use consumables. The upcoming NASA exploration programs to the Moon and Mars are based on concepts similar to the Apollo program: rendezvous and assembly of the transfer vehicle in earth orbit, followed by the command module orbiting the destination planet while humans go down to the surface. Assembly of the vehicles has so far depended on human control. Further, the Apollo program required one human to stay aboard the control module while others landed. By taking advantage of new technologies, it should be possible to enable autonomous assembly of the vehicles before humans get there, and to allow all humans to go down to the surface of the planets. Further, during a long-term flight, like those to Mars, having a satellite aid the humans inside the vehicle can be of benefit. These satellites could provide substantial support to maintain inventory, by being the ones that retrieve and re-stow items (therefore always keeping track of where supplies and equipment are located). The satellite could also enter areas that may become dangerous for humans in emergency cases. The ability of these types of satellites to provide useful help depends heavily on its ability to move around inside the larger spacecraft with ease and without worries that its propellant will run out.

The current long-term human presence in space is aboard the International Space Station (ISS). The crew has limited autonomous vehicles supporting them, basically limited to docking of Russian Progress cargo ships and the newer European ATV and Japanese HTV cargo modules. However, the crews are not aided inside the ISS by any robots. The SPHERES program [1], developed by the MIT Space Systems Laboratory is the only program currently aboard the ISS which operates free-flyer satellites. The project is advancing control algorithms for distributed satellites systems [3], including docking and in-space assembly [2]. However, the satellites must always operate under crew supervision for multiple reasons. One reason is that the satellites operate on cold-gas propellant, which is sufficient only for a few hours (~2h) of operation, after which the fuel tanks must be replenished by humans.

The challenges of propelling autonomous spacecraft have proven to be a major contributor to the cancellation of other past programs. These challenges include the need to operate solely on electricity (which can be easily replenished in space) without creating undue disturbances to the spacecraft or the environment.

An opportunity to demonstrate the development of a propellant-less system arose in 2008 as private astronaut Richard Garriott was headed to the ISS in October. While the opportunity did not materialize for an ISS test, several

[1] 978-1-4244-3888-4/10/$25.00 ©2010 IEEE.
[2] IEEEAC paper #11265, Version 2, Updated 2009:11:02

prototypes were designed and built between the Fall of 2008 and Spring 2009. In June 2009 these prototypes were validated aboard the ZERO-G reduced gravity airplane.

This paper present the results of this joint effort to develop a thruster based on an Ion-Drag Pump (IDP), which could operate as the main propulsion system for use in future satellites that operate in a pressurized environment. The concept of the engine is to remove the need for a fuel tank by floating inside the fuel. An IDP does have propellant, but it does not need it in a tank. It uses the air it floats in to create the thrust. The only other source of energy it needs is electricity, in order to ionize the air particles and create motion. Further, this propulsive system is advantageous due to the lack of moving parts.

Figure 1 illustrates the basic concept of operations for an IDP. High voltage is passed through a metallic needle (anode) which ionizes air molecules (Section A). The ions are then accelerated by an electric field and collide into non-ionized air molecules imparting momentum (Section B). The ions are then discharged at the grounded collection grid (cathode), and continue past the grid colliding with neutrals which are accelerated, creating thrust.

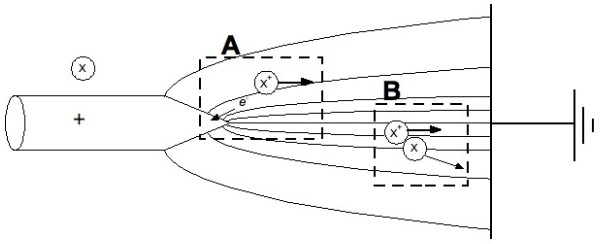

Figure 1 - Ion-Drag Pump thruster concept.

The primary limitation of the engine is its low thrust output. The goal of the research is to demonstrate that the thrust is sufficient to propel a helper satellite in micro-gravity. The prototype demonstration seeks to create a proof-of-concept and to identify any remaining limitations in making this technology a viable means of propulsion.

1.1 Experiment Overview

The intent of this experiment is validate the theory behind the design of a thruster based on an Ion-Drag Pump to a point where it would be practical for use aboard the ISS. An one-dimensional analytical model was developed to guide the design parameters. Several tests were conducted in the lab environment to finalize determination of the parameters, such as size and needle density. Measurement of the thrust of the test devices allowed assessment of the thrust to mass ratio. A circuit that operates on a single lithium AA battery was designed. A total of three prototypes of different sizes and densities were built to test aboard the ZERO-G plane. Figure 2 shows the large thruster ($8cm^2$) and the small thruster ($5cm^2$).

Figure 2. Two of the IDP Thrusters flown aboard the ZERO-G plane.

1.2 Theoretical Analysis of Ion-Drag Pumping

In [4] Kyle and Lozano used Steutzer's model [5], a unipolar theory for non-moving gases and insulating liquids. This is a well established theory that utilizes Maxwell's Stress Tensor and Gauss' Law. It is based upon a number of assumptions:

- the flow is steady, laminar and one-dimensional;
- the effect of gravity is neglected;
- the electric field distribution is one-dimensional and varies in the flow direction only;
- the space charge distributions conditions are saturated and determine field distribution and ion current flow;
- the diffusion current is lumped into the effective electrical conductivity of the fluid;
- the electrodes do not interfere with the fluid flow.

The decision to lump diffusion current into a constant conductivity factor simplifies the theory. Seyed-Yagoobi and Castañeda [6] expanded Steutzer's model to include current attributed to diffusion. The numerical solutions that they generated strongly agreed with experimental data. However, Lozano and Kyle's findings demonstrated that the decision to ignore diffusion does not affect the general trends when compared to experimental data (which holds true at the operations voltages of this experiment).

Steutzer's model can be manipulated to explicitly relate the thrust and voltage of the device, as seen in equations (1) and (2):

$$F = \frac{1}{2}\varepsilon_0 \left[\left(\frac{2\kappa\rho_0}{\varepsilon_0} \right)^2 \left(\sqrt{1+\frac{x}{\kappa}} - 1 \right)^2 \right] \cdot A \qquad (1)$$

$$V = \frac{1}{3}\frac{\varepsilon_0}{{\rho_0}^3}\left(\frac{i}{A\mu}\right)^2\left(\left(1+\frac{2A\mu{\rho_0}^2}{i\varepsilon_0}d\right)^{\frac{3}{2}}-1\right)+\frac{i}{A\rho_0}d \qquad (2)$$

or

$$\frac{V}{V^*} = -\left(\frac{d}{\kappa}-\frac{2}{3}\left[\left(1+\frac{d}{\kappa}\right)^{3/2}-1\right]\right), where: V^* = \frac{2\rho_0\kappa^2}{\varepsilon_0}$$

In both equations ε0 is vacuum permittivity, A is the cross sectional area of the device, i is the current, μ0 is ion mobility, ρ0 is space charge density, d is the distance between the plates, $\kappa = \frac{j\varepsilon_0}{2\mu\rho_0^2}$ and x is the distance between the needle tips and collection mesh. These equations were used to determine the design parameters and make an assessment of the experimental data.

Neither of these theories (Steutzer's and Castañeda's) explicitly define the space charge density at the anode. Space charge density refers to how much charge is being injected into the field and directly indicates how much current is able to run through the device. Equation (1) shows that the thrust increases with the square of the current. Therefore one objective of this experiment was to identify the limiting conditions of space charge density, which is critical in designing an optimum system.

Air Breathing Ion Engines - The process of using the atmosphere as a fuel source in electrostatic engines is known as an Air Breathing Ion Engine. Nishiyama has outlined how Air Breathing Ion Engines can lead to reduced mass of the propulsive system and propellant [7]. For a micro-satellite similar in size to the proposed concept (SPHERES) an Ion drag propulsion system can reduce the mass by over 50%.

While an Ion Drag propulsion system has advantages in mass reduction, Nishiyama also indicates that there are disadvantages. One major disadvantage is that the lighter the atoms or molecules being used as propellant of an IDP thruster, in this case air, the larger the diameter of the engine needed to increase the volume flow rate for a constant thrust.

Nishiyama found a positive correlation between thrust and the inlet area, assuming current density is held constant. Building upon these findings, the experiment also measured the effects of current density on thrust by using different needle configurations. An increase in thrust was expected as the needle density and area increased. However, these modifications also increased the mass of the system, which negatively effects the acceleration.

Needle-Mesh Electrode Configuration - One design variant of the Ion drag propulsion engine includes the use of needles on the ion emitter and a mesh at the collector. Yanada et al. outlined how increasing the number of needles attached to the emitter improves system performance [8]. Figure 3 shows Yanada's results, where H translates to thrust and n_E is the number of needles. This effect is diminished as the distance between the electrodes decreased.

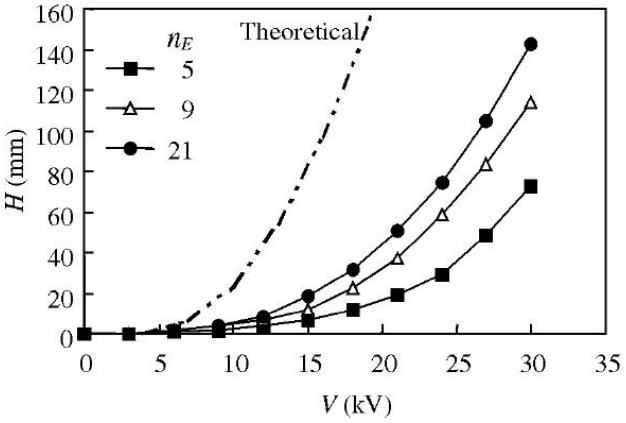

Figure 3 - Thrust-Voltage curve from Yanada.

Yanada also found that attaching needles to the collector electrode improves the performance of the propulsion system. Although adding collector needles increases the system performance, one major disadvantage is that the efficiency depends on the collector needle length. For collector mounted needles to have an effect, they must be longer than some yet undetermined limiting value. Yanada noted that further research is needed to determine it. Since this theory has not been experimentally confirmed, collector needles were not used in this project.

Yanada et al. states that the flow rate (thrust) of the system is a function of the number of emitter needles and the distance between the electrodes. Therefore, in order to increase the flow rate of the system, the number of needles should be maximal (up to the point of space charge saturation) while the distance between the electrodes should be minimal. The experiment assessed how needle density effects thrust against the cost of additional mass.

The theoretical development led to the determination of the following parameters:

- Needle dimensions (approximately 2.5-5cm long)
- Needle density (0.5-1.0 needles / cm^2)
- Cross sectional area ($5cm^2$ - $10cm^2$)
- Power (a few milli Watts)
- Voltage (3-20kV)
- Current (10-100 microA)
- Distance between plates (0.5-5cm)

2. THRUSTER DESIGN

The thruster consists of four main elements:

- Needles
- Emitter Plate
- Collector Place
- Electronic Circuit

These elements are described below.

2.1 Needle Manufacturing

The needles needed for the experiment were produced in the Space Propulsion Laboratory (SPL) at MIT. They were manufactured from 0.020" diameter tungsten wire that was purchased in straight 60" sections. The tungsten was cut into 1" sections using wire snips, creating a blank piece for each needle. A 1" PVC sleeve was slid onto the wire to ensure that all of the blanks were the same length, which was important for the etching process.

The etching apparatus consisted of a stand, a clamp, and a stainless steel cylinder submerged in a beaker filled with sodium hydroxide (NaOH 1 Normal). The process begins by inserting a blank into the clamp, with special care taken to ensure that the needle is at or near vertical. The clamp is then lowered using a graduated knob until the needle touches the surface of the NaOH. It is then lowered another 2 mm. It is important that the needle is placed in the center of the cylinder or the tip will not be symmetric, which is essential for the tip stability. A 35V potential is applied across the needle (anode) and cylinder (cathode) for two minutes. The capillary action of the sodium hydroxide causes a flow upwards towards the needle. As the base flows over the tip it removes mass, creating a fine tip. This process is illustrated in Figure 4.

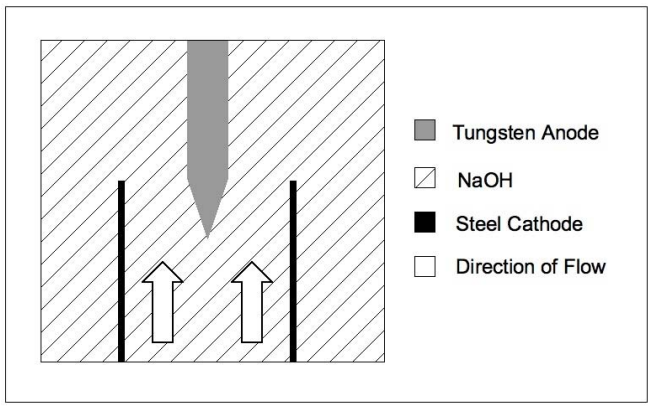

Figure 4 - Electrochemical etching process

The Materials Science Department at the University of Michigan has conducted a study on this electrochemical etching process and has reported achieving a radius of curvature at the tip of less than 100 nm. Figure 5 shows a scanning electron microscope image of a tip from their experiment. As discussed in the literature review, this scale of radius is essential for space charge saturation. As part of another project in the SPL, a needle made using the same process was viewed under an electron microscope with similar results.

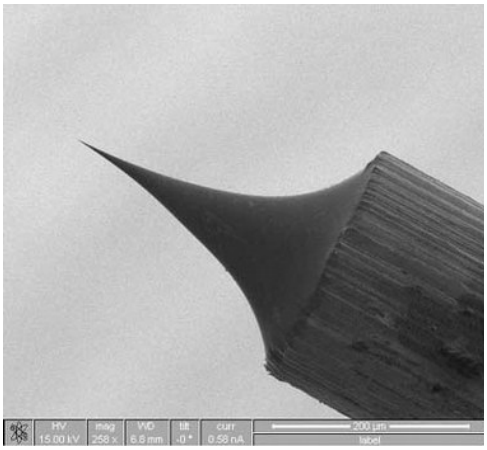

Figure 5 - Electron Scanning Microscope image of needle at 258x magnification (University of Michigan)

2.2 Emitter Plate

To minimize the mass of the system the plates were machined out of aluminum. It was necessary to use a metal due to the need for electrical conductivity. The final design of the 5cm emitter plate is shown in Figure 6.

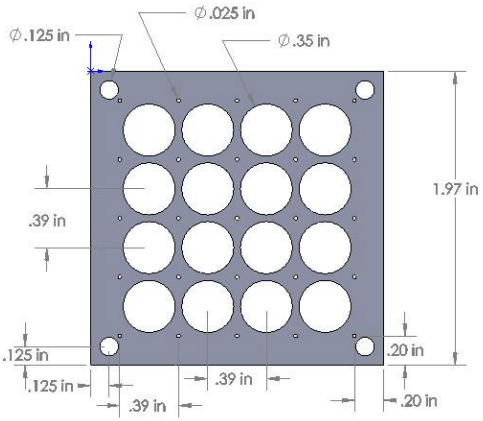

Figure 6 - Emitter plate design for smallest inlet area.

A waterjet was used to create the pieces from a 1/8" thick aluminum plate by cutting the outer edge of the plates and the air holes for all three plate sizes. The three dimensional mill was programmed to drill the .030" needle holding holes, the 1/8" rod holes, and the number 2 set screw holes. The set screw holes were then tapped. This process was repeated for the other two emitter plates as well, for a total of two $5cm^2$ plates and one $8cm^2$ plate.

Conductive silver epoxy was used to attach the needles to reduce the complexity of mounting the needles. An aluminum jig was used to hold the needles vertical while the epoxy was applied and set. The epoxy was viscous, allowing the needle tips to be moved until they were planar. The inner needles were placed first, followed by the outer needles. Once all of the needles had been placed, a heat gun was used to cure the epoxy.

To ensure even chargeflow, when measuring different densities, the needles needed to be placed symmetrically. Figure 7 shows the needle arrangement for the 5cm^2 plates.

2.3 Collector Plate

The outer dimensions and shape of the collector plate match those of the emitter plate and the removed inner area matches the perimeter of the needle holes on the emitter plate. This allows for the most direct flow of ions and air particles from the needle tips out the thruster. The collector plate also included an aluminum mesh, which was used to create the electric field of the thruster and collect the negative ions from the emitter plate. Figure 8 shows the design for the 5cm^2 collector plate.

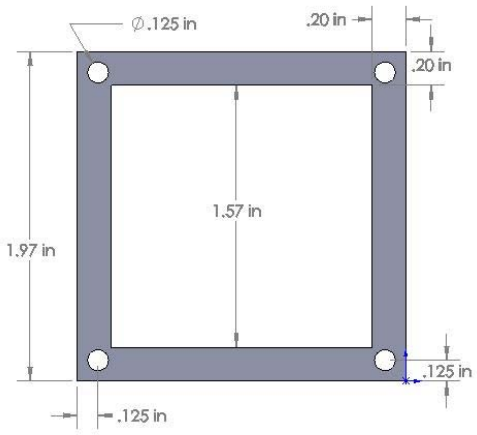

Figure 8 - Emitter plate design for smallest inlet area.

The aluminum mesh was cut to the correct size for each of the three pieces, and then bonded to the collector plate with conductive silver epoxy at 8 places.

2.4 Mechanical Part Integration

The final structural components are nylon rods and set screws that connect the base plates. Each prototype used four Nylon rods. Slotted round head number 2 set screws were used to fasten the plates to the rods and ensure their position was fixed during testing. The final structural configuration is shown in Figure 9.

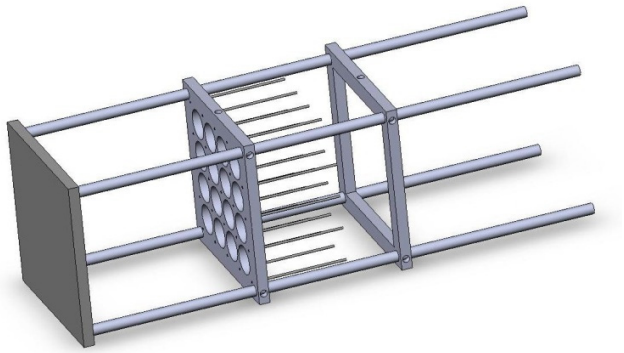

Figure 9 - Prototype structure

2.5 Electrical Circuit Fabrication

A main challenge of the project was the requirement to create a self-contained power source that could provide several kilo-volts with up to 100 micro-amps with minimum mass impact. Lithium thionyl chloride AA sized batteries were chosen to power the device because they provide the best amp-hour to mass ration while providing the power required by the engine. Increasing the voltage potential of these batteries (4 V) to a usable potential (10 kV) was done with commercial components. High performance direct current (DC) to high voltage direct current (HVDC) converters from EMCO High Voltage Power supplies were used to accomplish this. Two 5kV devices were run in series with a floating ground to create a 10 kV potential across the device. Two devices in series minimized the mass, since the single 10kV supplies have approximately

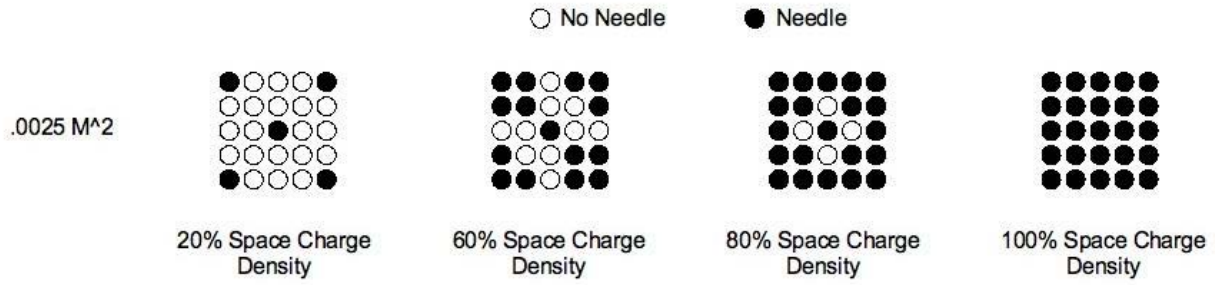

Figure 7 - Needle arrangement

four times more mass than the 5kV ones.

Because the voltage output of the DC-HVDC converters is a linear multiple of the input voltage, it was necessary to regulate the input voltage to a constant 5V input for each converter. This resulted in 5kV output at each converter, for the total of 10 kV between anode and cathode. A 5 V regulator evaluation kit from Maxim was used to regulate the battery voltage to a constant 5V. Prototyping tests confirmed the need for high capacity diodes in the final design; unfortunately these limited the output to 8 kV.

An RC timer delay circuit was also included so that the team could deploy the thrusters before they turn on, especially since the measurement equipment (a micro-scale) took several seconds to stabilize. A bypass switch was added to enable the team to turn the devices on immediately during ZERO-G flights.

The final circuit layout is shown in Figure 10. One version of the PCB created is pictured in Figure 11.

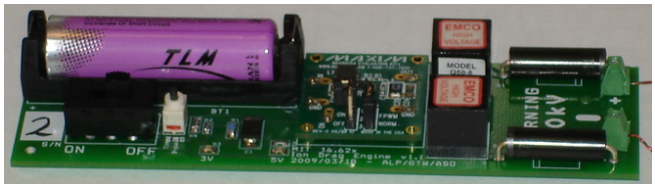

Figure 11 - DC-HVDC PCB

3. Experiment Plan

The testing variables for the experiment were separation between the needles and mesh collector, inlet area, and needle density. The separation between needles and mesh was tested first, independently of other variables. Table 1 presents the test matrix used for inlet area and needle density. The objective was to find the needle density first by building 5cm^2 plates with different densities. The space charge saturation does not change with inlet area; therefore it was possible to use one saturated density for all of the areas. Once the optimal needle density was determined, the 8cm^2 and 10cm^2 needle plates were built with that density.

Table 1 - Test matrix

Inlet Area [m^2]	Needle Density [needle/cm^2]			
	0.2	0.6	0.8	1.0
0.0025	X	X	X	X
0.0064	O	O	O	X
.01	O	O	O	X

The densities were chosen to encapsulate the expected asymptotic space charge curve. The size of an ISS "mid-deck locker equivalent" posed a limit of 10x10x20 cm for the volume of the device, which set the upper limit [9].

3.1 Laboratory Setup

Figure 12 depicts the laboratory testing setup. The specimen is being powered by the custom circuit described above (D), but in many of the tests a wall power source (A) was used to prevent unnecessary cost from battery usage. The power source was set to the same values as the IDP circuit.

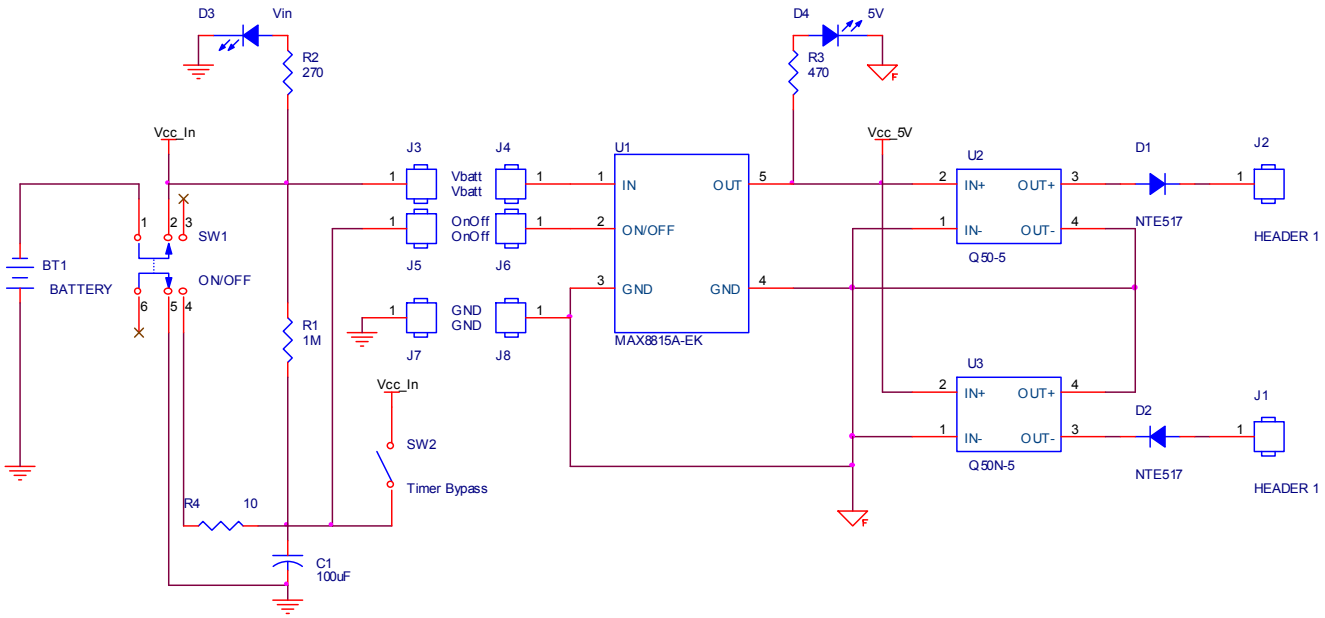

Figure 10 - DC-HVDC circuit design.

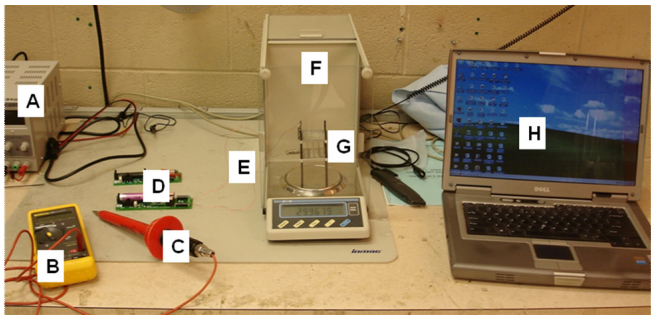

Figure 12 - Testing setup which includes the thruster, balance, and computer.

A voltmeter (B), accurate to 5%, was used with a high voltage probe (C) to verify the output voltage of the circuit. The probe can measure up to ±6000 V, accurate to 5%. The PCB's were connected to the thruster (G) using 30 gauge magnet wire (E) to minimize the structural and mass effects of the wire. The thrust of the propulsive system was measured with an Adam AAA 250L Analytical Balance (F). The balance measures to one-ten thousandth of a gram, two orders of magnitude smaller than the smallest expected measurement. It has a continuous output mode with produces data points at 10 Hz. The inlet section of the thruster points toward the scale. The specimen stands on the nylon rods, elevating the inlet off of the scale face. This configuration measures only the system thrust, as opposed to a thruster in the reverse orientation which would measure the effect of air being pushed onto the scale in addition to the system thrust. The balance was connected to a laptop computer (H) through an RS232 connection.

For each thruster variant the following procedure was used to procure 10 sets of data:

- STEP 0 Thruster: assemble and set the distance between the plates
- STEP 1 Balance: turn on and tare
- STEP 2 Thruster: place on scale
- STEP 3 Connect power source (still off)
- STEP 4 Start recording
- STEP 5 Turn on power source after 15 seconds
- STEP 6 Turn off power source after 20 seconds
- STEP 7 Stop recording after 15 seconds
- STEP 8 Repeat steps 4-7 at least once

3.2 ZERO-G Tests

The MIT SSL has substantial experience running tests aboard reduced gravity airplanes [11]. The team was further aided by Mr. Garriott's experience during training in similar flight. Therefore the team was ready to design the experiment for the hectic flight conditions. The primary considerations for the reduced gravity flight were:

- All tests must complete within 10 seconds
- It is not possible to measure absolute distance traveled with respect to the airplane frame of reference.
- At most 25% of the parabolas will provide useful results
- There exists substantial turbulence during "micro-gravity".

Based on these experiences the following design decisions were made:

- Based on the results from the lab experiments, *four* thrusters were tested:
- $5cm^2$ with 0.8 needles/cm^2
- $5cm^2$ with 1.0 needles/cm^2
- $8cm^2$ with 1.0 needles/cm^2
- A *control* (unactuated) thruster which will show the motion of the airplane
- A deployment mechanism to deploy all the specimens at the same time was designed.

During each parabola all of the specimens were to be deployed, and the difference in distance traveled (in the direction of thrust) between the control and the actuated units would allow us to determine the thrust created by the engines. The deployment system is pictured in Figure 13. It consisted of two "plates" made from foam core (non-conductive) which were shaped to hold all four specimens in place. During the "2g" time the specimens were positioned for deployment. As micro-gravity time started, the upper plate was lifted out of the way (since most of the parabolas had up motion), and the lower plate was left almost motionless while the thrusters "lifted off" from it. The control was set in the center, resulting in a "V" formation of the thrusters, which allowed us to compare the distance traveled during micro-gravity time.

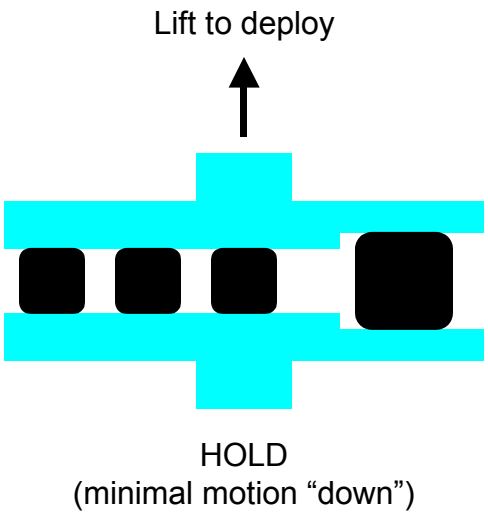

Figure 13. Deployment Mechanism

4. RESULTS

This section introduces the data and explains the analysis methods used. First, a sample of raw data is explained. Next, the parameters are explored: plate separation; four density tests and their relevance to space charge density; and the three inlet area test specimens. This data is then converted into expected distance traveled by each device in 10 seconds and the error analysis is explaind. The results of the ZERO-G flight are presented last, and compared with the expected values from laboratory tests. Important information about the performance of the thrusters was gained at every level of the data analysis.

4.1 Raw Data

Figure 14 shows an example of the raw data recorded from one of the experiment runs. The first region of the graph (A) indicates the recorded mass for the thruster when the power was turned off. Similarly, region (D) is the time period after the device has been turned off. This was measured to ensure that the balance did not deviate during measurement. The findings showed that the average values for sections (A) and (D) were always within 0.1%. The average of these two measurements was used as the structural mass.

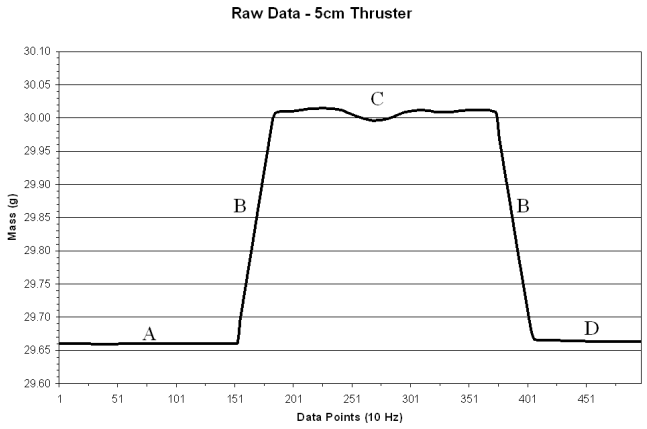

Figure 14 - Data from 5cm^2 100% test

Sections (B) indicate the period from when the power source was turned on/off and until the balance stabilized. Unfortunately, the rising and falling sections do not give useful information about the thruster response time. The sharp corners and linear nature of these sections is due to the response time of the scale, listed by the manufacturer as 3 seconds. In all cases there are approximately 30 data points on the rise and fall, or 3 seconds. To implement this type of thruster, accurate information about the response time and overshoot will be needed for dynamic control.

Section (C) represents the period of time when the thruster is powered. This was registered as an increased mass reading. The raw data were used to calculate the thrust produced by the IDP thruster using equations (3) and (4). m_{pwr} is the average mass reading across section (C) and m_{unpwr} is the average mass readings across sections (A) and (D). Using an acceleration of 9.8 m/s2 for gravity, it is possible to calculate the average thrust for each run in Newtons.

$$\Delta m = m_{pwr} - m_{unpwr} \quad (3)$$

$$Thrust \quad = F = \Delta m \cdot a \quad (4)$$

The resulting average thrust for this run was 3.34 mN.

4.2 Plate Separation

The first test was to confirm the separation between the plate and the needles. The theory from (1) and (2) indicates that it is desired to have the needles close to the mesh[3]. However, there are physical limitations. As the voltage rises, the air conductivity becomes relevant, until a "breakdown" occurs and arcs form between the needles and the mesh. These arcs do not produce any thrust, and therefore are undesirable[4]. Figure 15 shows the results of the plate separation tests. The experimental breakdown of air was reached sooner than the theoretical one, limiting the separation of the place to approximately 0.7cm. While the ideal situation is to place the plates as close as possible (the exponential theoretical gain), a separation distance of approximate 0.8cm was selected to prevent arching. The curve shows that the experimental data closely matches the expected theoretical values, validating this part of the model.

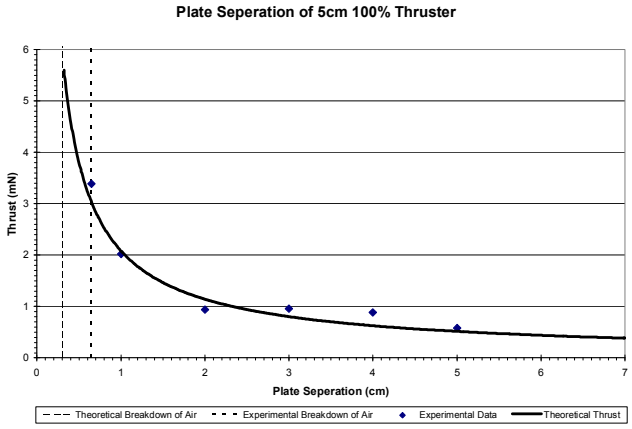

Figure 15 - Theoretical ideal thruster separation

[3] The core equation is (1), which shows that thrust increases explicitly with spacing (x); however κ, which depends on current density (j) and charge density (ρ), plays an important role. In the space charge limited regime, j decreases with larger spacing as x^{-2}, and ρ increases linearly with j. The net effect in (1) is that the term x/κ turns into something proportional to 1/x, and the ρ^2 term becomes something close to $1/x^4$. Therefore the rapid rise in thrust when reducing the spacing.

[4] The breakdown of air is also affected by the humidity of the environment. This was not a problem aboard the ZERO-G plane. However, during humid summer days arcing in laboratory tests was experienced.

4.3 Needle Density

The purpose of the needle density tests was to identify the space charge saturation point in terms of needles per centimeter. This is the point at which an increase in needle density offers a negligible increase in thrust. The density tests were conducted with the 5cm^2 plates first to identify this point so that the larger plates could be populated at the correct density.

Table 2 shows the results of the varying needle density experiments. From this table, it is clear that the saturation point has been reached by 0.8 needles/cm^2 density. This is pertinent to the design of future engines - the next generation of thrusters will not need to include more than .8 needles/cm^2. Figure 16 shows the asymptotic thrust-density curve with confidence intervals. As predicted, the curve is asymptotically approaching 3.5 mN. The larger confidence interval for the 1.0 needles/cm^2 density engine may explain why the average thrust was slightly lower than the 0.8 needles/cm^2 density engine. The small error bars (not greater than ±0.06 mN) show that the thrust produced by these devices at a given voltage is repeatable. This is an important characteristic for a usable thrust system.

Table 2 - Thrust vs Needle density

Needle Density [needle/cm^2]	0.2	0.6	0.8	1.0
Thrust [mN]	1.61	2.57	3.34	3.33

Although the values for the thrust at a given density may be skewed by the sensitivity in the distance between the plates, the values for 0.8 and 1.0 density are each within 10% of the asymptote value. Because these points are within 1% of each other and particularly close to the asymptotic value, one can still assert that the saturation point occurs in this needle density range.

4.4 Inlet Area

The decision was made to populate the larger thrusters at 1.0 needles/cm^2 to ensure operation above the saturation point. This would compensate for any possible errors made when recording the density data. The added mass of the needles was negligible, below 1g (compared to over 100g for the complete system). Table 3 shows the results of the varying inlet area tests.

Table 3 - Thrust vs Area

Area [cm^2]	5	8	10
Density [needle/cm^2]	1.0	1.0	1.0
Thrust (mN)	3.33	6.62	7.06

The first two data points gave the expected results. Specifically, they increased linearly from zero. Figure 17 shows these points with the theoretical line.

The data from the 10cm^2 plate falls short of its expected thrust by more than 50%. This was determined not to be a failure of the theory; rather it is an equipment failure. Specifically, the HV DCDC converters have reached their current limit in this case. The measured output current of the converters it was 0.125 mA, which is 25% greater than the rated maximum output current listed in the

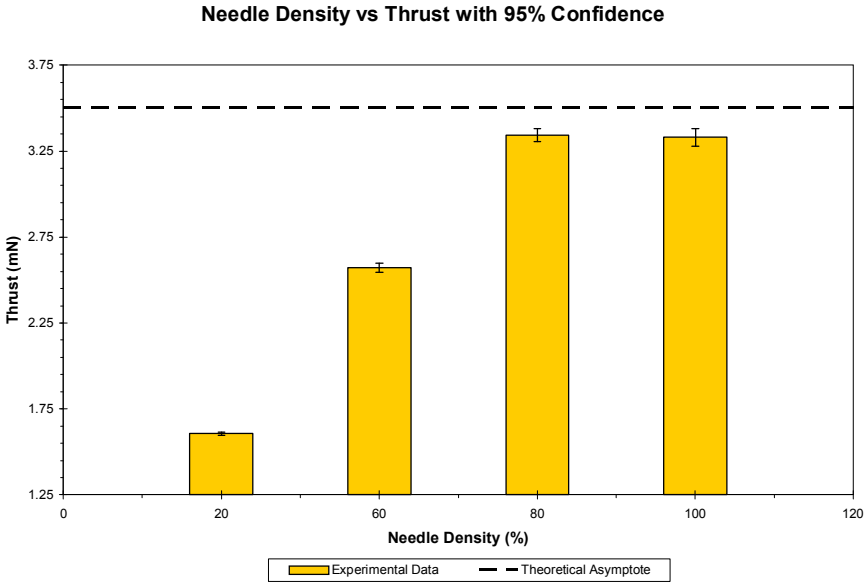

Figure 16 - Density vs Thrust with Confidence Intervals

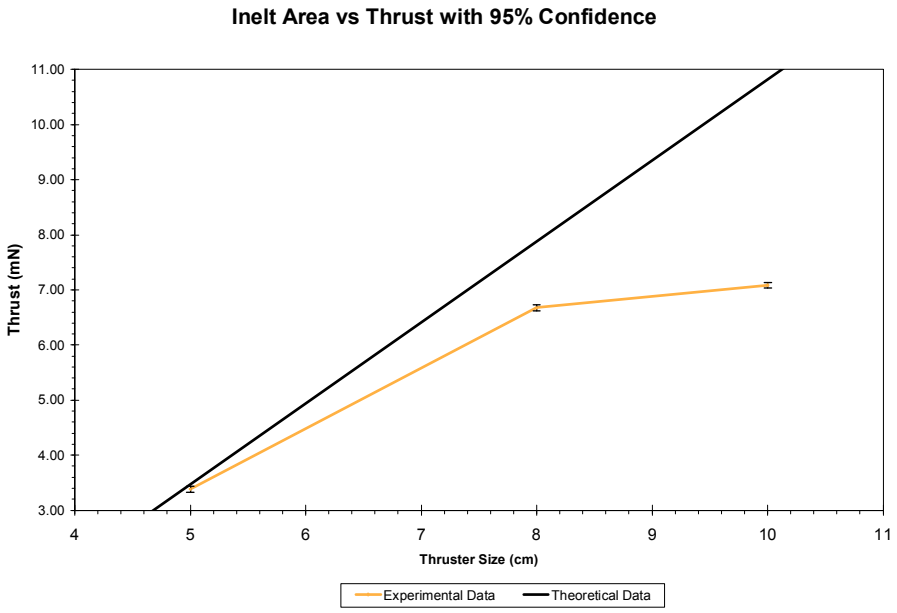

Figure 17 - Inlet Area vs Thrust with Confidence Intervals

manufacturers data sheet [10]. It reached this maximum current when the voltage had only been increased to 7 kV. A more robust power supply should enable the 10cm^2 plate to produce the full 11 mN of thrust. Extrapolating from the other two points, shows the expected current requirement for the 10cm^2 plate to be 0.19 mA in order to operate at full capacity. Due to the inability of the circuit to drive the 10cm^2 plate, it was not used for the ZERO-G flights.

As with the density tests, the error bars for this data are small (on the order of ±.05 mN). Again this means that the devices produce consistent thrust when plate distance and voltage are held constant. Unlike the density tests, as the thrust increased the error bars got smaller. This is another indication that the device has been limited at or before 7 mN. The device is straining itself to output 7.06 mN nearly every time.

4.5 Distance Travel Calculation

The goal of the laboratory development was to create a system that can propel itself the equivalent of its body length in 10 seconds, to obtain relevant results in the ZERO-G flights. With a known force for each test specimen and a time constraint, it was possible to approximate how far they would travel in a microgravity environment. Equations (5) and (6) were used to calculate the acceleration for each specimen. This acceleration was then used with Equation (7) to calculate the theoretical distance traveled. It is worth noting that this calculation ignores several unknown effects that relate to air resistance. The device may act differently if it is operating in airflow.

$$m_{system} = m_{structure} + m_{circuit} \qquad (5)$$

$$a_{thruster} = \frac{Thrust}{m_{system}} \qquad (6)$$

$$d = \frac{1}{2} a_{thruster} \cdot t^2 \qquad (7)$$

Table 4 and Figure 18 show the results of this calculation for the devices that were run. Inspection shows that even the most poorly performing device exceeded performance standards by more than 6 times. In tests, the best device was the 8cm^2 plate which was expected to travel 23.1 times farther than hypothesized. In terms of applicability, the 8 cm thruster would be able to move a 500 g payload half a meter in 10 seconds.

These results are specific to the power supply; if this can be improved, then the 10cm^2 plate would likely outperform the rest. Also, a "helper" would likely be larger (in both volume and mass) than any of the thrusters. In this case, designers would want to use the largest inlet area possible combined with a voltage higher than 10kV.

4.6 Error Analysis

There are two different error sources in the experimental data: scale (bias error) and air currents (random error). The scale error was ignored for this analysis since the manufacturer stated it was ±0.0001g, which is less than 1% of the significant measurements. Since the error due to air currents was immeasurable, this analysis considered the error to be normally distributed within the mass measurements. Equations (8-11) were used to determine the error in the measurements and confidence intervals.

Table 4 - Expected Distance Traveled in 10 Seconds by Each Configuration.

Specimen	System Mass [g]	Length [cm]	Thrust [mN]	Distance Traveled [m]	Distance Traveled/Length
5 cm 20%	90	0.103	1.61	0.9	8.7
5 cm 60%	91	0.103	2.57	1.4	13.6
5 cm 80%	92	0.103	3.34	1.8	17.5
5 cm 100%	92	0.103	3.33	1.8	17.5
8 cm 100%	101	0.143	6.62	3.3	23.1
10 cm 100%	160	0.143	7.06	2.2	15.4

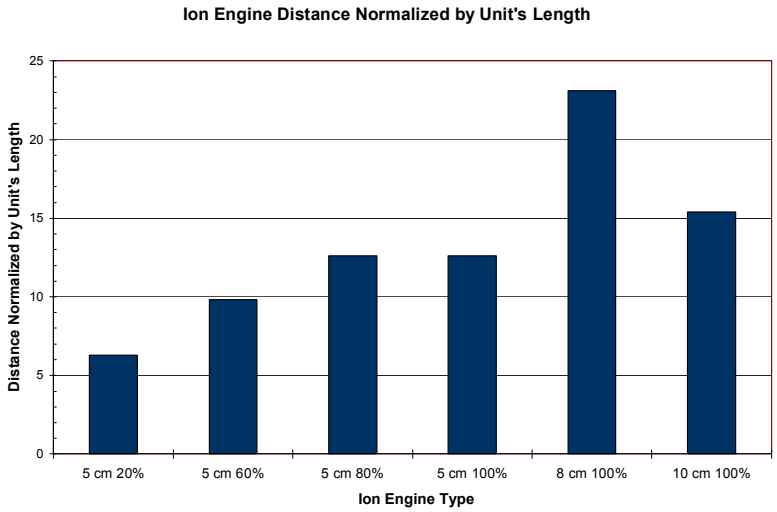

Figure 18 - Normalized distance traveled for all configurations

$$\bar{x} = \frac{\sum_{i=1}^{n} x_i}{n} \tag{8}$$

$$s = \sqrt{\frac{\sum_{i=1}^{n} (x_i - \bar{x})^2}{n-1}} \tag{9}$$

$$\mu = \bar{x} - t_{\alpha/2,n-1} \frac{s}{\sqrt{n}} \tag{10}$$

$$\mu = \bar{x} + t_{\alpha/2,n-1} \frac{s}{\sqrt{n}} \tag{11}$$

Equation (8) calculates the mean thrust estimator for the IDP thruster trials, where n is the number of trials and x is the average thrust for that trial. Equation (9) uses the result of Equation (8) to calculate the estimate for the standard deviation of the IDP thruster between the trials. The result of Equation (9) was then passed into Equation (10) and Equation (11) to determine the upper and lower value of the thrust with a 95% confidence limit. In these equations $t_{\alpha/2,n-1}$ is the two tailed t-test value, which is found in a t-table dependent on the number of trials and the confidence level desired. For this experiment, t-test value based on the number of trials per IDP thruster variant and the 95% confidence level is 2.622.

Using the aforementioned equations, Table 5 contains the confidence interval results for the IDP thruster variants. Thrust confidence represents the distribution between the trials of each thruster and states what values a given trial should occur within. According to the calculation, there is 95% confidence that the average thrust produced by a device will fall within last two values of Table 5.

4.7 ZERO-G Results

The IDP Thrusters were tested aboard the ZERO-G reduced gravity airplane (2009-June-21). The flight was shared among multiple research groups, therefore there were only eight micro-gravity parabolas attempted. There were also six lunar gravity and six Martian gravity parabolas

Table 5 - Thrust Mean, Std Dev, Lower Limit and Upper Limit for all Configurations

Thruster	5cm 20%	5cm 60%	5cm 80%	5cm 100%	8cm 100%	10cm 100%
Thrust Mean ($\bar{x}$)	1.61	2.57	3.34	3.33	6.62	7.06
Thrust Std Dev (s)	0.01	0.04	0.05	0.07	0.08	0.03
Thrust Confidence+ (μ)	1.60	2.54	3.30	3.28	6.56	7.03
Thrust Confidence- (μ)	1.61	2.60	3.38	3.38	6.67	7.08

performed (the thrusters were not able to create any motion even in lunar gravity).

As predicted from previous experience, of the eight micro-gravity parabolas three had successful runs. All the other parabolas had too much turbulence and the thrusters collided with a wall or other people within on second of leaving the deployment mechanism.

Video analysis of the parabolas provided the results shown in Table 6. The experiments aboard the Zero-G plane were recorded using two high definition video cameras mounted to the wall. Images from these cameras were used to quantify the experimental results. Screenshots were taken from the least turbulent trial at a rate of 5 Hz. For each still frame, a key line was drawn along the edge of each thruster. This captured information about both the position and orientation of the thrusters throughout the flight. Each thruster was given a key color: 8cm^2 - red; 5cm^2 / 1.0 - blue; 5cm^2 /0.8 - green; control - white/black.

The results were obtained by using the length of the control thruster (10cm) as a reference during video analysis, and using the video time frame to calculate the time of useful motion. As shown in the table, the time that the thrusters could actuate before they had contact with the airplane or people was only a few seconds. The limited time did not allow them to move "20 times their length" as predicted for 10s parabolas. However, their motion in two seconds was representative of the expected thrust.

Figure 19 shows a screen capture of one run. At deployment the 5cm^2 / 1.0 needles/cm^2 specimen (right end) is approximately 2/3 of a body ahead of the control (second in from right to left). Detailed frame-by-frame studies show that after 1.5 seconds the unit is fully ahead of the control, meaning it traveled approximately 4.75cm. The 5cm^2 specimens have a mass of 154g. This equates to a thrust of approximately 6.5mN. The expected thrust was 3.3mN.

Table 6 - ZERO-G Results

Trial	Thruster	Distance	Time	Thrust
1	5cm^2 / 0.8	6cm	2s	5mN
2	5cm^2 / 1.0	4.75cm	1.5s	6.5mN
3	5cm^2 / 1.0	7.5cm	2s	8mN
3	8cm^2 / 1.0	14.3cm	2s	11.0mN

Figure 20 shows a detailed video analysis of trial 3. The key lines were averaged to find the average orientation during flight. The dot product of $\vec{r}$ and $d\vec{r}$ gives the number of body lengths each thruster moved in the average direction of thrust. The displacement vector for the 8cm^2 thruster was within one degree of its average direction of thrust, while the 5cm^2/1.0 was off by 22 degrees. This motion leads to the conclusion that the displacement was caused almost entirely by thrust from the thrusters. Lambda is the average of the tracking lines over the two seconds. The 8cm^2 specimen traveled its full length of 14.3cm (λ=1.0); the 5cm^2/1.0 traveled ~7.5cm (λ=0.75 for a length of 10cm); the 5cm^2/0.8 did not provide good results in this run.

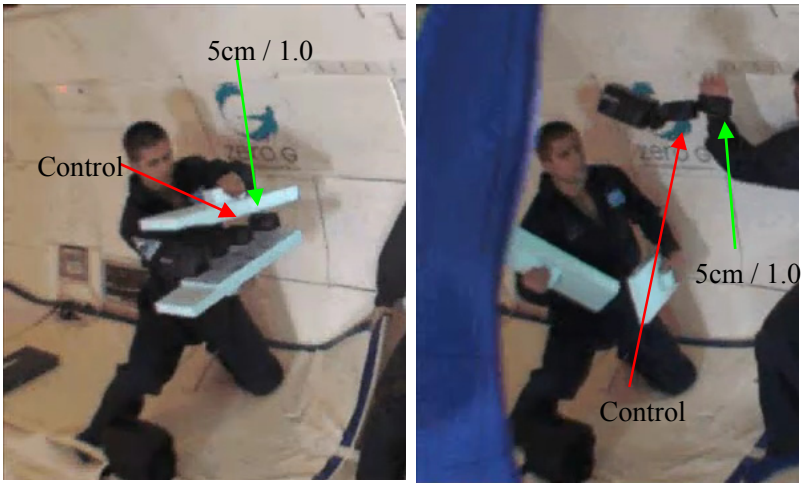

5cm Ion Engine starts 2/3 a body length ahead of the control.

5cm Ion Engine is one body length (~14.3cm) ahead of the control after ~1.5s.

- Distance traveled ~4.75cm
- Time ~1.5s
- Mass = 154 g

-> Thrust ~6.5mN.

Figure 19 - ZERO-G Results show the 5cm thruster ahead of the control.

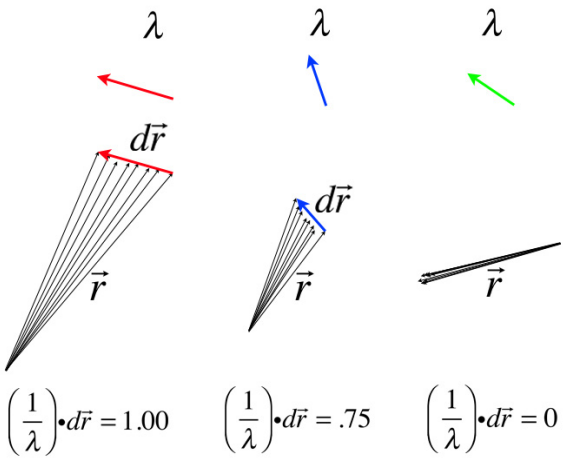

Figure 20 - Detailed analysis of a ZERO-G trial

A summary of the ZERO-G results versus the expected results from laboratory tests is presented in Table 7. All the thrusters performed better than expected during the ZERO-G tests. However, the ZERO-G measurements have large margins of error, especially due to the inability to measure true distance traveled in the direction of thrust. Therefore, it is possible to conclude that a proof-of-concept has been demonstrated to operate in 6DOF, and that it can in fact propel its own length well within 10 seconds. The fact that the ZERO-G thrust and the expected laboratory thrust are well within an order of magnitude of each other demonstrates the validity of the development process. Further, it does leave open the possibility that test a longer than approximately 5 seconds would provide substantially better data to corroborate the laboratory findings.

Table 7 - ZERO-G versus Laboratory Thurst

Specimen	Laboratory	ZERO-G	Difference
$5cm^2$ / 0.8	3.32mN	5mN	+50%
$5cm^2$ / 1.0	3.33mN	6.5-8mN	+96%
$8cm^2$ / 1.0	6.62mN	20.1mN	+203%

5. CONCLUSIONS

This experiment aimed to explore whether a self contained Ion-Drag Pump thruster could produce sufficient thrust to move its body length in a given amount of time. To accomplish this goal, several different IDP thruster variants were fabricated based on analysis from a one dimensional model. The thrusters were then connected to a power source and tested to determine which thruster type met the performance criteria. The best performing thrusters were tested aboard the ZERO-G reduced gravity airplane.

Three different design variables were tested: plate separation, needle density, and inlet area. The plate separation was mostly a test of the air breakdown before arcing occurred, since the separation should be minimized according to the theory. Varying needle density allowed determination of the space charge saturation point as being approximately 0.8 needles per square centimeter. However, only one other measurement was taken (at 1.0 needles/cm^2), which means there is the possibility of better precision in finding the saturation point. It was demonstrated that thrust increases linearly with area, verifying Steutzer's model. The experimental results showed this to be true when the electrical system was able to provide the necessary power. In this case the trend between $5cm^2$ and $8cm^2$ was as expected; however, it was not possible to demonstrate this for a $10cm^2$ due to the electronics limitations.

From these experiments it was possible to determine that all the IDP thrusters types were able to perform to the criteria for ZERO-G flight: travel their own distance within 10s. The largest ratio of distance traveled to length would be in the $8cm^2$ 1.0 needles/cm^2 thruster case, which was 23.1; the smallest ratio occurred in the $5cm^2$ / 0.2 needles/cm^2 case, which was 6.3 body lengths.

The ZERO-G flights provided periods of microgravity smaller than expected, at only approximately 2 seconds. However, video analysis of the tests, and using the control as a guide, it was possible to determine that the thrust of the stand-alone units is similar to that seen in the laboratory environment. This is promising to the technology, as further advances in electronics could soon provide the necessary power for a unit that could be of help to crews aboard the ISS and future long-term missions.

5.1 Suggestions for Future Work

Although the IDP thruster variants were able to produce enough thrust to propel itself its body length, this experiment demonstrated the need for further investigation into this technology. The following points outline possible suggestions for future work on the IDP thruster concept.

The existing models are mostly based on 1-D analysis. However, the shape of the area might play an important role, especially because of boundary effects. Similarly, the lack of analytical 2D models prevents a good prediction of current density saturation points. Therefore, further theoretical work remains on the modeling of these systems.

A clear area of future work is in the development of electronics that can provide higher power (current) at high voltages (beyond 10kV). This would enable large area thrusters to be operational and potentially provide close to the same thrust as SPHERES thrusters (100mN), which have proven to be sufficient for reasonable motion aboard the ISS.

The inability of the scale to correctly measure the response time of the thruster leaves for future work the creation of a dynamic model of the thrusters. To correct for this issue, a

balance that has a faster response time should be used when measuring the change in mass. Additionally, the balance's level of precision was greater than needed – less precise balances typically have faster response times.

The thrust is an exponential function of the plate separation. The most sensitive region of this graph is between the electrical breakdown of air at 10,000 V (0.33cm) and 1cm. To increase the understanding of the relationship between the thrust and plate separation additional data should be taken in this region with a greater focus on precision measurement.

Finally, the experiment was limited to operate without motion control. If these devices are implemented in space modules, the airflow seen at the inlet will be different. The effects of drag and disturbance could present significant performance control problems. Innovative airfoils and control surfaces will have to be studied to make this technology practical for autonomous vehicles.

6. REFERENCES

[1] Enright, J, Hilstad, MO, et al, "The SPHERES Guest Scientist Program: Collaborative Science on the ISS", 2004 IEEE Aerospace Conference (Paper #1296), Big Sky, Montana, March 7-12, 2004

[2] Fejzic, A, et al, "Results of SPHERES Microgravity Autonomous Docking Experiments in the Presence of Anomalies", 59th International Astronautical Congress, Sep-Oct 2008

[3] Saenz-Otero, A, et al, "Distributed Satellite Systems Algorithm Maturation with SPHERES Aboard the ISS", 59th International Astronautical Congress, Sep-Oct 2008

[4] Kyle, J, and Lozano, P, "Ion Drag Pump Propulsion Implementation for SPHERES," MIT Summer Research Program, 2008.

[5] Steutzer, O. M., "Ion Drag Pumps," Journal of Applied Physics, Vol 31, 1960, pp. 136.

[6] Seyed-Yagoobi, J. and Castañeda, J., "Theoretical Analysis of Ion-Drag Pumping," IEEE Transactions on Industry Applications, Vol 31, No 3, 1995, pp. 469-476.

[7] Nishiyama, K., "Air Breathing Ion Engine Concept," 54th International Astronautical Congress of the International Astronautical Federation, the International Academy of Astronautics, and the International Institute of Space Law 29 September - 3 October 2003, Bremen, Germany, IAC-03-S.4.02.

[8] Yanada, H., el al., "An investigation of an ion drag pump using a needle-mesh electrode configuration," Journal of Mechanical Engineering Science, Vol 216, Part C, 2002, pp. 325-335.

[9] "ISS User's Guide - Release 2.0", NASA, Houston TX, 2000.

[10] "Ultra-Miniature DC to HV DC Converters," EMCO High Voltage Corporation, CA, April 2009. [http://www.emcohighvoltage.com/ Accessed 4/13/2009]

[11] Saenz-Otero, A, Chen, A, et al, "SPHERES: Development of an ISS Laboratory for Formation Flight and Docking Research", 2002 IEEE Aerospace Conference, #081, March 9-16, 2002

7. BIOGRAPHY

Alvar Saenz Otero *is a Research Scientist at the MIT Aeronautics and Astronautics Department / Space Systems Laboratory. He is the lead research scientist of the SPHERES program. His research concentrates on development of facilities for technology maturation, space systems engineering, and avionics research. He previously worked on the Origins testbed, part of NASA's NGST program, in the development of automatic optical alignment. He has PhD in AeroSpace Systems, and MEng and BS degrees in Electrical Engineering and a BS degree in Aero/Astro, all from MIT.*

Alexander Pina *participated in this program while a senior undergraduate student at the MIT Department of Aeronautics and Astronautics as part of his experimental design course. He is now a Systems Engineer at MIT Lincoln Laboratory. At MIT he also conducted research for the MIT AgeLab, where his research concentrated on secondary task overload during driving. He holds a BS degree in Aerospace Engineering, June 2009.*

Greg Wellman *participated in this research program while a senior undergraduate student at the the MIT Department of Aeronautics and Astronautics as part of his experimental design course He is now a Second Lieutenant in the US Army's Aviation Branch. He has been identified as a member of the Army's Space Cadre and is considering a career with the Army in Space Operations. Greg received his BS in Aero/Astro from MIT.*

Paulo Lozano *is the Charles Stark Draper Assistant Professor of Aeronautics and Astronautics. His main interests are plasma physics, space propulsion, ion beam physics, small satellites and nanotechnology. In 2007, he received MIT's Karl Chang Innovation award for his work in electrochemical microfabrication on porous metals and in 2008 was awarded through the Young Investigator Program Award by the AFOSR for his work in electrospray thrusters. He has published over 40 conference and journal publications and teaches subjects in space and rocket propulsion, fluid mechanics and plasma physics. He holds a PhD in Space Propulsion from MIT (2003).*

Richard Garriott *is currently Vice-Chairman of Space Adventures, which includes ventures in Zero-G Corporation, the X-Prize, and Spacehab. He was a Private Astronaut during October 2008, spending 12 days aboard the International Space Station, which helped inspire the research presented in this paper. He is a software programmer by profession.*